Journal of Alloys and Compounds 520 (2012) 213–219

Contents lists available at SciVerse ScienceDirect

Journal of Alloys and Compounds

journal homepage: www.elsevier.com/locate/jallcom

Preparation, characterization and enhanced visible light photocatalytic activities of polyaniline/Bi_3NbO_7 nanocomposites

Weiming Wu, Shijing Liang, Lijuan Shen, Zhengxin Ding, Huarong Zheng, Wenyue Su, Ling Wu*

State Key Laboratory Breeding Base of Photocatalysis, Research Institute of Photocatalysis, Fuzhou University, Fuzhou 350002, PR China

ARTICLE INFO

Article history:
Received 23 July 2011
Received in revised form
26 December 2011
Accepted 4 January 2012
Available online 12 January 2012

Keywords:
Polyaniline/Bi_3NbO_7
Nanocomposites
Chemical synthesis
Photocatalysis

ABSTRACT

Polyaniline/Bi_3NbO_7 nanocomposites were successfully prepared by a simple chemisorption approach. Their particle sizes ranged from 25 to 50 nm. The photocatalytic activities of the as-prepared samples for the rhodamine B degradation were evaluated under visible light (420 nm $\leq \lambda \leq$ 760 nm). The results indicated that the samples exhibited excellent photocatalytic activities and high activity stabilities for the degradation of rhodamine B. When the loading amount of polyaniline was 4 wt%, the obtained sample showed the highest photocatalytic activity. Its photocatalytic activity was also much higher than that of the reference sample ($TiO_{2-x}N_x$ powders). On the basis of the experimental results, photo-generated holes were detected as the main oxidation species responsible for the decomposition of rhodamine B over polyaniline/Bi_3NbO_7. Furthermore, the enhanced photocatalytic activity was mainly ascribed to the synergetic effect between polyaniline and Bi_3NbO_7.

1. Introduction

Photocatalysis has received considerable attention because of its promising applications such as in photocatalytic degradation of organic pollutants [1,2] and photocatalytic splitting of water [3,4]. In order to efficiently utilize sunlight, the development of visible light driven photocatalysts becomes a hot topic in photocatalysis scopes [5–10]. Bismuth-containing materials, such as Bi_2MO_6 (M = Mo or W) [9,10], $BiVO_4$ [11] and $PbBi_2Nb_2O_9$ [12], have attracted much attention in the photocatalysis field because of their excellent visible-light photocatalytic activities. Furthermore, nanosized bismuth-containing photocatalysts have been synthesized using soft-chemical processes, such as solvothermal routes [10,13,14], ultrasonic-assisted method [15] and citrate complex process [16]. These compounds have showed relatively higher performances in the photocatalytic reactions compared to their bulk counterparts with the same chemical composition due to the unique physical and chemical properties of nanoparticles [17]. Bi_3NbO_7, which has a band gap of about 2.8 eV, is a good candidate as visible light driven photocatalyst. Recently, nanosized Bi_3NbO_7 photocatalysts have been reported to show photocatalytic activities for the degradation of organic pollutants and hydrogen evolution from water splitting under visible light irradiation [18,19]. However, the performances of Bi_3NbO_7 in the photocatalytic reactions are still unsatisfactory.

Polyaniline (PANI) is known as a good conductive polymer [20]. Furthermore, it is also regarded as an efficient photogenerated holes-transporting material, which can facilitate the separation of photo-generated electron–hole pairs and can promote interfacial electron transfer process [21]. In previous papers, based upon the synergetic effect between PANI and photocatalysts, rapid charge separation and slow charge recombination were came true [22–25]. The visible or/and ultraviolet photocatalytic activities of photocatalysts were remarkably enhanced by the modification of PANI, such as PANI/TiO_2 [22], PANI/ZnO [23], PANI/CdS [24] and PANI/$BiVO_4$ [25]. Therefore, the introduction of PANI is expected to great enhance the visible light photocatalytic activity of Bi_3NbO_7.

Herein, PANI/Bi_3NbO_7 nanocomposites were successfully prepared by the simple chemisorption approach. Their photocatalytic activities for the rhodamine B degradation were evaluated under visible light. The degradation process of rhodamine B over PANI/Bi_3NbO_7 nanocomposites was studied in detail. Furthermore, the probable photocatalytic mechanism under visible light irradiation was also proposed.

2. Experimental

2.1. Materials and reagents

The following materials and reagents were used as starting materials: citric acid monohydrate ($C_6H_8O_7 \cdot H_2O$, A.R., Sinopharm Chemical Reagent Co. (SCRC)), ammonia solution (NH_3 (aq.), *ca.* 25 wt%, SCRC), nitric acid (HNO_3 (aq.), 65–68 wt%, SCRC), niobium ammonium oxalate ($NH_4H_2[NbO(C_2O_4)_3] \cdot 3H_2O$, 20.7% in Nb, H.C. Starck), hydrogen peroxide (H_2O_2 (aq.), 30 wt% solution in water, SCRC), bismuth nitrate pentahydrate ($Bi(NO_3)_3 \cdot 5H_2O$, A.R., SCRC) and PANI (Polyaniline, Alfa Aesar Co.).

* Corresponding author. Tel.: +86 591 83779362; fax: +86 591 83779105.
E-mail address: wuling@fzu.edu.cn (L. Wu).

0925-8388/$ – see front matter © 2012 Elsevier B.V. All rights reserved.
doi:10.1016/j.jallcom.2012.01.021

2.2. Preparation

Bi_3NbO_7 nanoparticles were prepared *via* a *sol–gel* method: a mixture of niobium ammonium oxalate (0.01 mol, 4.47 g), $Bi(NO_3)_3{\cdot}5H_2O$ (0.03 mol, 14.55 g) and citrate acid (0.08 mol, 16. 80 g) was dissolved in 30 mL of H_2O_2 (aq.). After adding 2 mL of HNO_3 (aq.), the mixture was heated at 65 °C for 1 h to decompose oxalate within niobium ammonium oxalate. Then, the pH value of the solution was adjusted to about 6.5 by dropping NH_3 (aq.) to obtain a yellowy solution. The precursor solution turned into a resin-like gel with a high viscosity by heating at 120 °C for several hours. The gel was treated at 300 °C for 2 h to burn out unnecessary organics, and then calcined at 550 °C for 2 h to obtain yellow Bi_3NbO_7 powders.

PANI/Bi_3NbO_7 nanocomposites were synthesized by the simple chemisorption approach: a certain amount of PANI and 0.1 g of Bi_3NbO_7 nanoparticles were mixed in 10 mL of tetrahydrofuran, sonicated for 5 min, and stirred for 18 h. Then, the mixture was removed from the solvent and was dried at 120 °C for 2 h. According this process, PANI/Bi_3NbO_7 samples with different PANI mass ratios of 2, 4 and 6% were synthesized, respectively.

2.3. Characterizations

X-ray diffraction (XRD) patterns were collected on a Bruker D8 Advance X-ray diffractometer with a Cu Kα radiation. The data were recorded in the 2θ range of 20–80°. UV–vis diffuse reflectance spectra (UV–vis DRS) were obtained on a Cary 500 UV–vis–NIR spectrophotometer. $BaSO_4$ was used as a reflectance standard. Mott–Schottky measurement was performed at a Zenuium electrochemical workstation (Zahner Co.). For Mott–Schottky experiment, the potential ranged from 0 to 1.0 V (*vs.* Ag/AgCl, pH 6.6), and the perturbation signal was 10 mV with the frequency of 1, 3 and 5 kHz, respectively. X-ray photoelectron spectroscopy (XPS) measurement was carried out by using a VG Scientific ESCA Lab Mark II spectrometer equipped with an Mg X-ray source ($h\upsilon$ = 1253.6 eV). The binding energy (BE) calibration of the spectra was referred to C 1s peak located at BE = 284.6 eV for the analysis. Transmission electron microscopy (TEM) images were measured by a FEI Tencai 20 microscope at an accelerating voltage of 200 kV. Samples for TEM were prepared by placing a drop of the sample suspension on a copper grid coated with carbon film and dried in the atmosphere. FTIR spectrum on a pellet of the sample mixed with KBr (m_{sample}:m_{KBr} = 1:10) was recorded by a Nicolet Nexus 670 FT-IR spectrometer at a resolution of 4 cm^{-1}.

2.4. Photocatalytic test

For the photodegradation of rhodamine B (RhB), an ozone-free 300 W Xe lamp (PLS-SXE300, Trusttech Co. Ltd., Beijing, intensity: ~700 mW cm^{-2} at λ = 420 nm) with a cutoff filter of 420 nm and an infrared filter was used as the light source (420 nm ≤ λ ≤ 760 nm). The initial concentration of RhB was 1×10^{-5} M. In the catalytic test, 50 mg of catalyst was suspended in 50 mL of RhB solution in a 100 mL glass beaker. Before the test, the suspension was stirred in the dark for 2 h to ensure the establishment of adsorption–desorption equilibrium between the catalyst and RhB. As the reaction proceeded, 3 mL of the suspension was taken at 1 h intervals and was centrifuged. The concentration of RhB was analyzed by monitoring the height of the maximum absorbance (λ = 554 nm) in UV–vis absorption spectra with a Cary 50 UV–vis spectrophotometer (Varian Co.). For comparison, the degradation of RhB over $TiO_{2-x}N_x$ powders was also performed according to the same procedure. $TiO_{2-x}N_x$ powders were prepared by treating P25 powders (Degussa Co.) in the NH_3 atmosphere at 550 °C for 3 h [6].

3. Results and discussion

3.1. XRD patterns

XRD patterns of the as-prepared samples are shown in Fig. 1. All diffraction peaks of the patterns agree well with a cubic Bi_3NbO_7 (space group *Fm*-3*m* (225)). The main peaks at 2θ value about 28.19°, 32.66°, 46.86°, 55.59°, 58.29°, 68.44°, 75.59° and 77.92° are assigned to the diffraction peaks of the (111), (200), (220), (311), (222), (400), (331), (420) and (422) planes, respectively. Furthermore, the XRD pattern of PANI (4 wt%)/Bi_3NbO_7 is similar with that of Bi_3NbO_7, implying that the crystal structure of Bi_3NbO_7 is intact after modified by PANI.

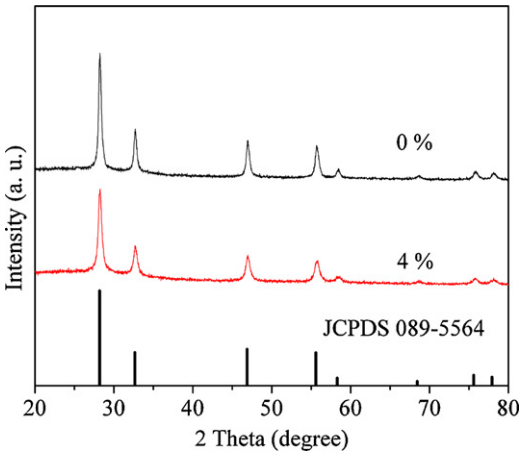

Fig. 1. XRD patterns of Bi_3NbO_7 and PANI (4 wt%)/Bi_3NbO_7.

3.2. UV–vis DRS analysis

Fig. 2 shows the UV–vis DRS spectra of Bi_3NbO_7 and PANI (4 wt%)/Bi_3NbO_7. In generally, the wavelength at the absorption edge for a semiconductor is determined as the intercept on the wavelength axis for a tangential line drawn on the absorption spectrum. Therefore, the absorption edges of Bi_3NbO_7 and PANI (4 wt%)/Bi_3NbO_7 locate at 452 and 466 nm, corresponding to band gaps of about 2.74 and 2.66 eV, respectively. A red shift of the band gap transition is observed. This indicates that the modification of PANI improves the utilization of visible light for Bi_3NbO_7, which may enhance the photocatalytic activity of Bi_3NbO_7.

3.3. Mott–Schottky measurement

The flat-band potential is obtained from Mott–Schottky plots (taken in the dark) for Bi_3NbO_7 using the following equation [26]:

$$\frac{1}{C^2} = \left[\frac{2}{\varepsilon\varepsilon_0 eN}\right]\left[E - E_{ef} - \frac{kT}{e}\right]$$

where C is the capacitance of space charge, ε is the dielectric constant of semiconductor, ε_0 is the vacuum permittivity, e is the elementary charge (+*e* for electrons, −*e* for holes), k is the Boltzmann constant, T is the absolute temperature and E_{ef} is the flat-band potential.

As shown in Fig. 3, Bi_3NbO_7 shows the characteristic behavior of an n-type semiconductor because of the positive slope of the linear plots. The flat-band potential came from the extrapolation for $C^{-2} = 0$ is *ca.* −1.0 V *vs.* Ag/AgCl at pH 6.6 for Bi_3NbO_7. Therefore, the band structure of Bi_3NbO_7 can be roughly evaluated based on the combination of band gap and flat-band potential [27]: the redox

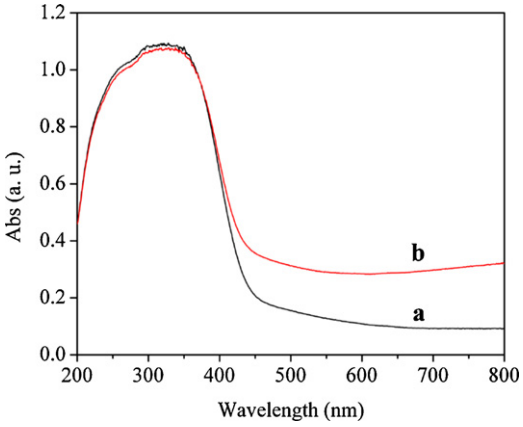

Fig. 2. UV–vis DRS spectra of (a) Bi_3NbO_7 and (b) PANI (4 wt%)/Bi_3NbO_7.

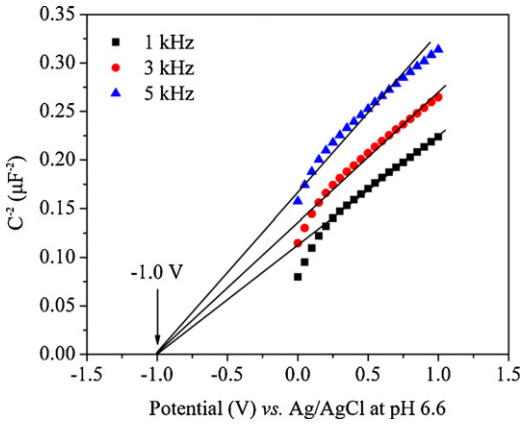

Fig. 3. Mott–Schottky plots for Bi_3NbO_7.

potentials for the top of the valence band and the bottom of the conduction band are −1.00 and 1.74 V, respectively.

3.4. Morphologies

Fig. 4(a) and (c) shows TEM images of the typical samples (Bi_3NbO_7 and PANI (4 wt%)/Bi_3NbO_7). The particle sizes of the samples range from 25 to 50 nm, indicating the nanocrystalline nature of the samples. The fringes of $d = 0.32$ nm are clearly observed in the HRTEM images (Fig. 4(b) and (d)). This matches well with that of the (1 1 1) crystallographic plane of Bi_3NbO_7, which is the strongest crystallographic plane in the XRD pattern. Furthermore, the HRTEM image (Fig. 4(d)) reveals that Bi_3NbO_7 particles are surrounded by a small amount of PANI. The thickness of the PANI layer is about 0.7 nm.

3.5. XPS analysis

XPS spectra of Bi_3NbO_7 are shown in Fig. 5. The scan survey spectrum demonstrates that the sample is composed of Bi, Nb, O and C elements. The presence of carbon element comes from the hydrocarbon contaminants, which commonly exists for XPS. Therefore, the obtained sample is a pure Bi_3NbO_7, which is in agreement with the XRD analysis result. Characteristic binding energy values of 164.0 eV and 158.6 eV for Bi $4f_{5/2}$ and Bi $4f_{7/2}$ reveal a trivalent oxidation state for bismuth [18]. The binding energy at 209.1 and 206.3 eV for Nb $3d_{5/2}$ and Nb $3d_{3/2}$ can be assigned to an Nb^{5+} oxidation state [28]. The high-resolution XPS spectrum of O 1s core level line is composed of two peaks: (1) the energy binding of O 1s (529.6 eV) is closely associated with the lattice oxygen (O_L); (2) the binding energy peak at 531.1 eV can be assigned to the loosely bound oxygen (O_A) on the sample surface, such as adsorbed O_2 or H_2O.

3.6. FTIR spectra

Fig. 6 shows the FTIR spectra of the samples. The main characteristic bands of PANI (Fig. 6(b)) are assigned as follows: the bands at about 1563 and 1481 cm^{-1} are attributable to the C=N and C=C stretching modes for the quinoid and benzenoid rings, respectively [23,29]. A C—N stretching mode for benzenoid ring

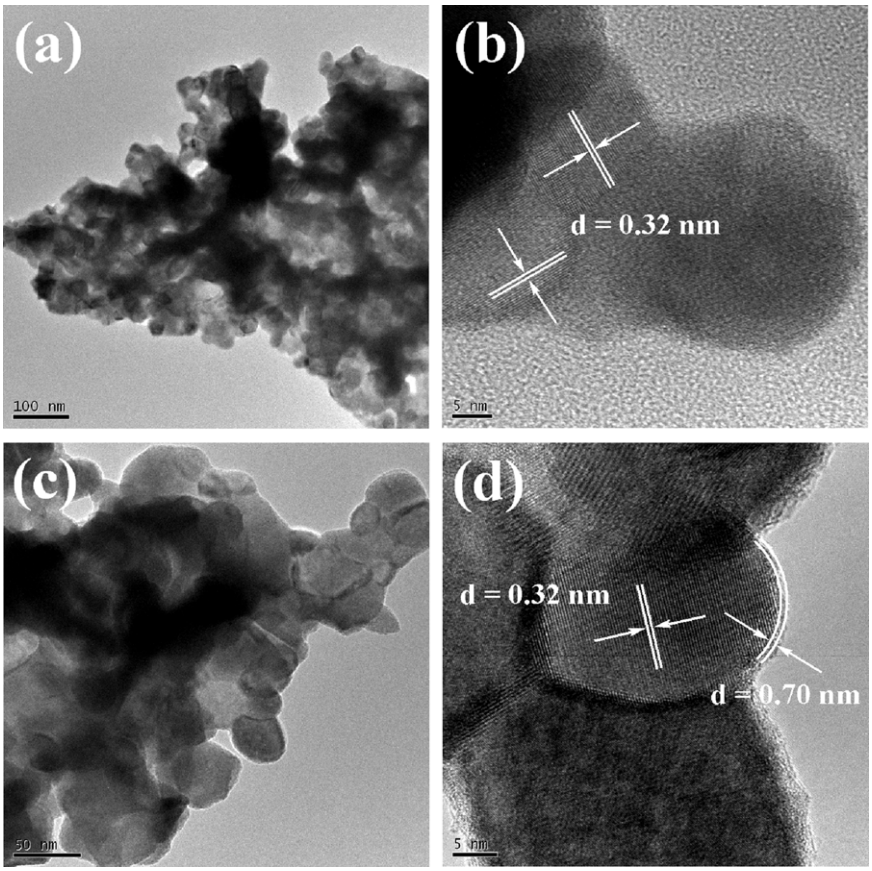

Fig. 4. TEM and HRTEM images for the as-prepared samples: (a) TEM and (b) HRTEM images for Bi_3NbO_7, and (c) TEM and (d) HRTEM images for PANI (4 wt%)/Bi_3NbO_7.

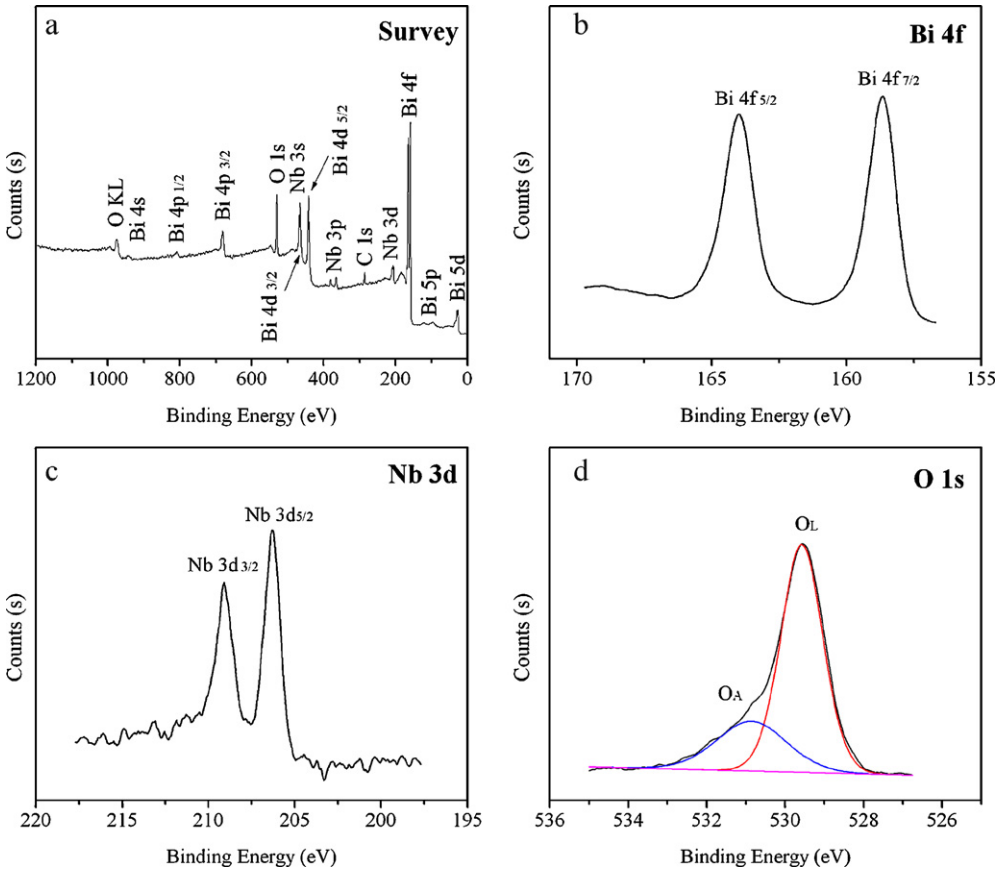

Fig. 5. (a) The XPS survey spectrum of Bi_3NbO_7 and the high-resolution XPS spectra of (b) Bi 4f and (c) Nb 3d and (d) O 1s for Bi_3NbO_7.

is observed at around 1291 and 1240 cm^{-1} [22,29]. The peak at about 1111 cm^{-1} is assigned to the in-plane bending vibration of C—H [29]. As compared to PANI, several characteristic bands of PANI bonded on the surface of the Bi_3NbO_7 nanoparticles (Fig. 6(c)) shift to higher wavenumber. Such peak shifting is mainly ascribed to the interaction between PANI and Bi_3NbO_7. This chemical interaction may cause high efficiency of charge separation and induce synergetic effect to enhance the photocatalytic activity of Bi_3NbO_7.

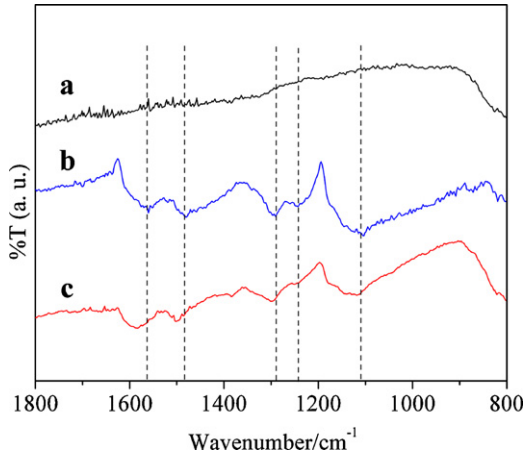

Fig. 6. FTIR spectra of (a) Bi_3NbO_7, (b) PANI and (c) PANI (4 wt%)/Bi_3NbO_7.

3.7. Photocatalytic activities

The photocatalytic activities of the as-prepared samples for the degradation of RhB are evaluated under visible light (Fig. 7). It is found that the introduction of PANI greatly enhances the photocatalytic activity of Bi_3NbO_7. The photocatalytic activity of PANI/Bi_3NbO_7 initially increases with the increase of the loading amount of PANI. When the PANI content is 4 wt%, the obtained sample shows the highest photocatalytic activity. Its photocatalytic activity is also much higher than that of the reference sample ($TiO_{2-x}N_x$ powders). However, further increasing the loading amount of PANI, the photocatalytic activity decreases gradually though it remains higher than that of bulk Bi_3NbO_7. This reveals that the optimal PANI loading amount is 4 wt%. Furthermore, it is noted that the mechanical mixture sample of PANI (4 wt%) and Bi_3NbO_7 exhibits negligible photocatalytic activity. Therefore, it may be concluded that the loading amount of PANI and the synthetic method of PANI/Bi_3NbO_3 have pronounced effects on the photocatalytic activities of the as-prepared samples.

For the activity stability, the photocatalytic activity of PANI (4 wt%)/Bi_3NbO_7 does not obviously decrease in the whole recycle experiment (Fig. 8). In addition, the results of XRD and FTIR reveal that no significant changes are observed in the crystal structure and surface chemical compositions of the sample before and after the catalytic reaction (Fig. 9). These results indicate that the photocatalyst possesses high activity stability.

In order to identify the main active species for the RhB degradation over PANI/Bi_3NbO_7, several scavengers have been employed in

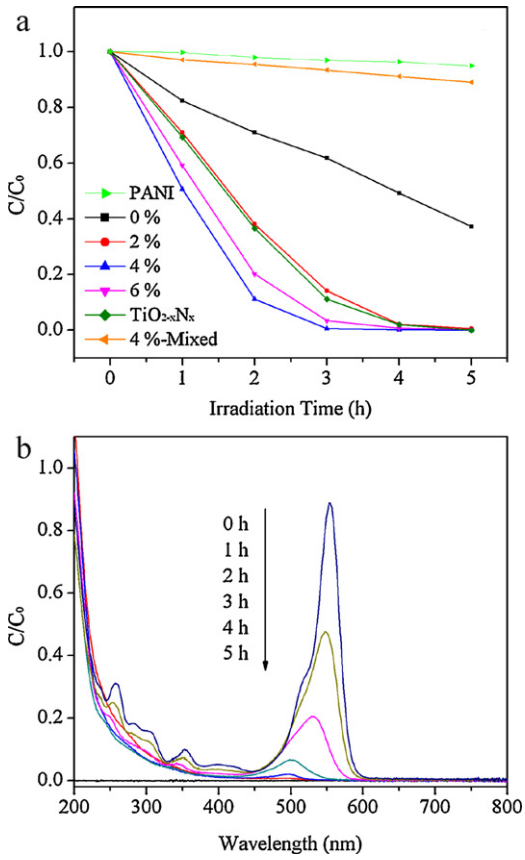

Fig. 7. (a) Concentration changes of RhB over PANI/Bi_3NbO_7 samples and $TiO_{2-x}N_x$ powders under visible light irradiation and (b) UV–vis absorption spectrum of RhB over PANI (4 wt%)/Bi_3NbO_7.

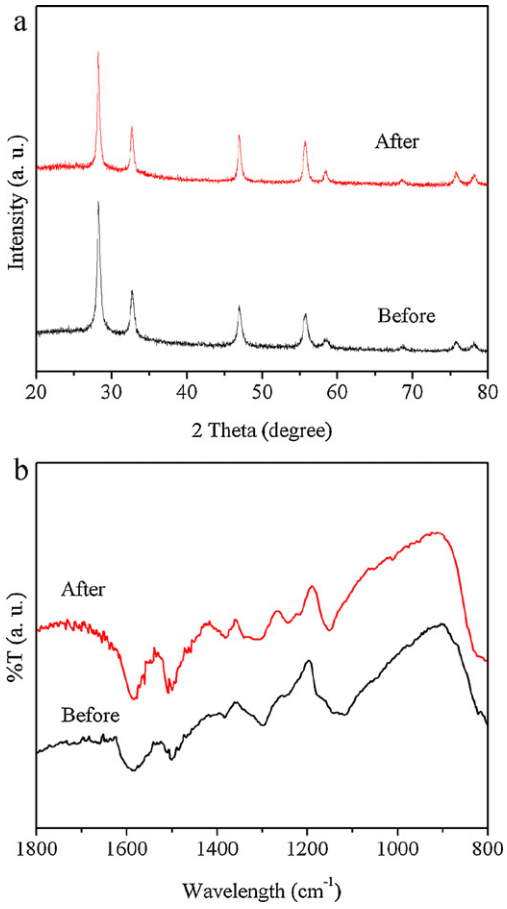

Fig. 9. (a) XRD patterns and (b) FTIR spectra of PANI (4 wt%)/Bi_3NbO_7 before and after the catalytic reaction.

the photocatalytic reaction process: ammonium oxalate for holes [30], isopropanol for •OH radicals [31] and potassium dichromate for electrons [32]. As shown in Fig. 10, the photocatalytic activity of the as-prepared sample is greatly reduced in the presence of ammonium oxalate. However, the photodegradation ratio of RhB only slightly changed by the addition of isopropanol. Furthermore, the photocatalytic activity is enhanced in the presence of potassium dichromate upon purging with nitrogen. The enhanced photocatalytic activity can be ascribed to the high separation efficiency of electron and hole pairs. Therefore, these results suggest that the decomposition of RhB by PANI/Bi_3NbO_7 is mainly ascribed to the oxidation of the holes instead of •OH or/and $•O_2^-$ radicals.

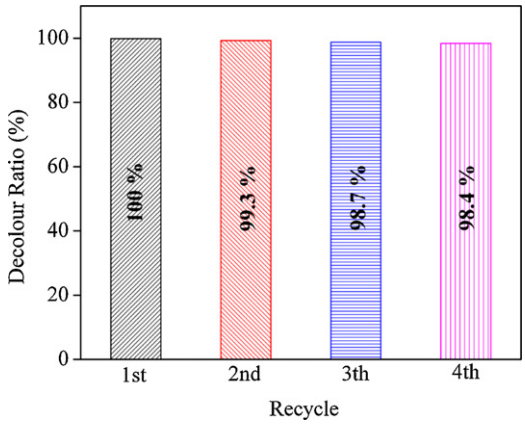

Fig. 8. Reuse of PANI (4 wt%)/Bi_3NbO_7.

On the basis of the above experimental data, the enhanced photocatalytic activity is mainly ascribed to the high efficiency of charge separation induced by the synergetic effect between PANI and Bi_3NbO_7. The redox potentials of PANI (LUMO and HOMO [21,29]) and Bi_3NbO_7 (conduction band (CB) and valence band (VB)) are shown in Fig. 11: the CB of Bi_3NbO_7 is lower than the LUMO of PANI, so the former can act as an electron acceptor; the VB of Bi_3NbO_7 is lower than the HOMO of PANI, so the later can act as a sink for photo-generated holes. This reveals that PANI and Bi_3NbO_7 match well in energy level, which can cause the synergetic effect. As shown in Fig. 11, both PANI and Bi_3NbO_7 absorb visible light to generate hole-electron pairs. Due to the synergic effect, the excited state electrons in the LUMO of PANI can readily inject into the CB of Bi_3NbO_7, and then react with oxygen molecules to product $•O_2^-$ radicals ($O_2/•O_2^-$, 0.48 V *vs.* Ag/AgCl [33]). Simultaneously, the photo-generated holes in the VB of Bi_3NbO_7 can emigrate to the HOMO of PANI easily and oxidize the adsorbed RhB directly (RhB/RhB*, 0.55 V *vs.* Ag/AgCl [34]), since PANI is a good photogenerated hole-transporting material [20]. In summary, the synergic effect between PANI and Bi_3NbO_7 facilitates the separation of photo-generated electron-hole pairs and promotes interfacial electron transfer process. Thus, the photocatalytic activity of Bi_3NbO_7 photocatalyst is greatly enhanced by the introduction of PANI.

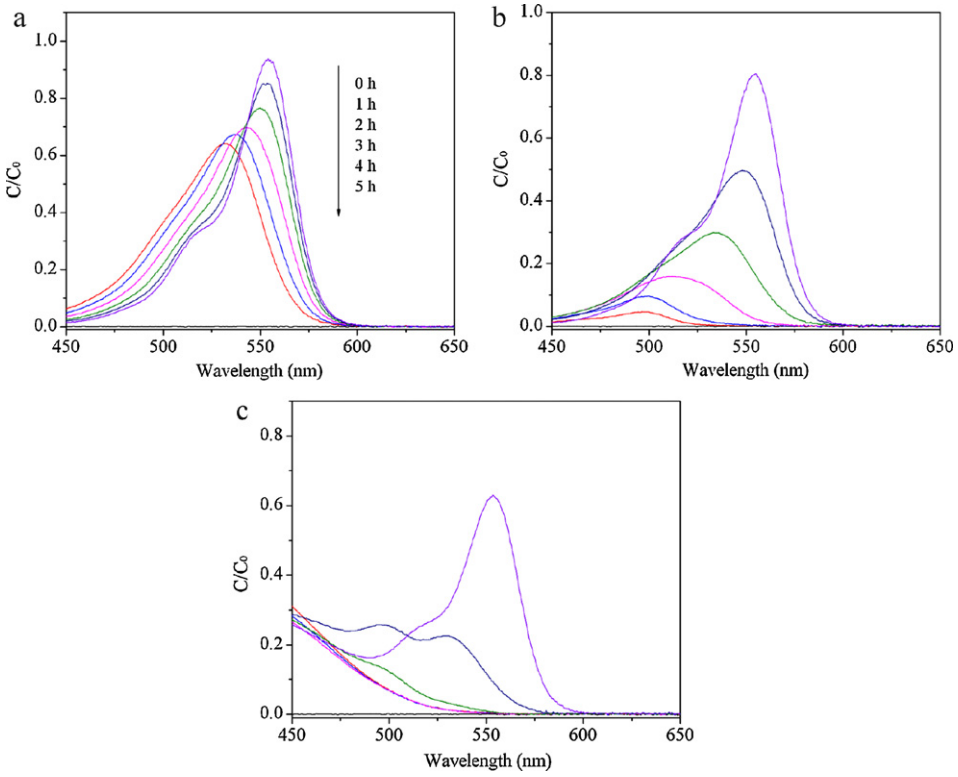

Fig. 10. Variations in the concentration of RhB over PANI (4 wt%)/Bi_3NbO_7 in the presence of different scavengers: (a) 1.5×10^{-2} mol L^{-1} of ammonium oxalate, (b) 1.5×10^{-2} mol L^{-1} of isopropanol and (c) 5.5×10^{-4} mol L^{-1} of potassium dichromate with N_2 (40 mL/min).

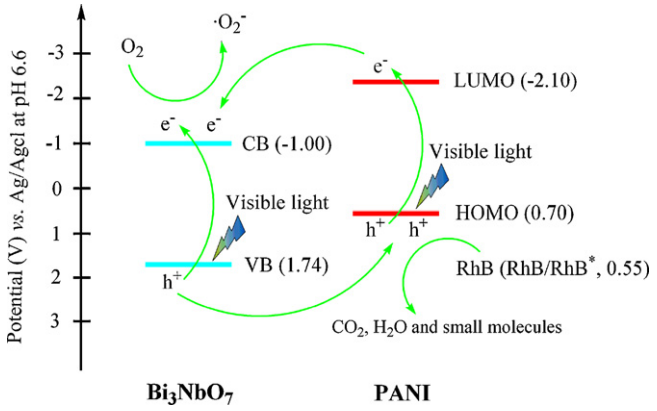

Fig. 11. Probable degradation process of RhB over PANI/Bi_3NbO_7 nanocomposite.

4. Conclusions

PANI/Bi_3NbO_7 nanocomposites were successfully prepared *via* the simple chemisorption approach. The particle sizes of the obtained samples ranged from 25 to 50 nm. The introduction of PANI greatly enhanced the photocatalytic activities of the obtained samples for the RhB degradation under visible light irradiation, due to the high efficiency of charge separation induced by the synergetic effect between PANI and Bi_3NbO_7. Further experiments indicated that PANI/Bi_3NbO_7 had high activity stability for the decomposition of RhB. It was also found that the loading amount of PANI and the synthetic method had pronounced effects on the photocatalytic activities of the as-prepared samples. The optimal PANI loading amount was 4 wt%. Furthermore, photo-generated holes were detected as the main oxidation species responsible for the RhB degradation over PANI/Bi_3NbO_7.

Acknowledgements

The work was supported by the National Natural Science Foundation of China (21177024 and U1033603), the Natural Science Foundation of Fujian Province, China (2011J01041 and 2010J01033), the National Key Basic Research Program of China (973 Program: 2011CB612314) and the Program for Changjiang Scholars and Innovative Research Team in University (PCSIRT0818).

References

[1] M. Wu, A. Sápi, A. Avila, M. Szabó, J. Hiltunen, M. Huuhtanen, G. Tóth, Á. Kukovecz, Z. Kónya, R. Keiski, W. Su, H. Jantunen, K. Kordás, Nano Res. 4 (2011) 360–369.
[2] Z. Liu, X. Zhang, S. Nishimoto, T. Murakami, A. Fujishima, Environ. Sci. Technol. 42 (2008) 8547–8551.
[3] A. Fujishima, K. Honda, Nature 238 (1997) 37–38.
[4] H. Kato, K. Asakura, A. Kudo, J. Am. Chem. Soc. 125 (2003) 3082–3089.
[5] S.U.M. Khan, M. Al-Shahry, W.B. Ingler Jr., Science 297 (2002) 2243–2245.
[6] R. Asahi, T. Morikawa, T. Ohwaki, K. Aoki, Y. Taga, Science 293 (2001) 269–271.
[7] X. Wang, K. Maeda, A. Thomas, K. Takanabe, Gang Xin, J.M. Carlsson, K. Domen, M. Antonietti, Nat. Mater. 8 (2009) 76–80.
[8] Z. Yi, J. Ye, N. Kikugawa, T. Kako, S. Ouyang, H. Stuart-Williams, H. Yang, J. Cao, W. Luo, Z. Li, Y. Liu, R.L. Withers, Nat. Mater. 9 (2010) 559–564.
[9] Y. Shimodaira, H. Kato, H. Kobayashi, A. Kudo, J. Phys. Chem. B 110 (2006) 17790–17797.
[10] L. Wu, J. Bi, Z. Li, X. Wang, X. Fu, Catal. Today 131 (2008) 15–20.
[11] A. Kudo, K. Omori, H. Kato, J. Am. Chem. Soc. 121 (1999) 11459–11467.
[12] H.G. Kim, D.W. Hwang, J.S. Lee, J. Am. Chem. Soc. 126 (2004) 8912–8913.
[13] J. Bi, L. Wu, J. Li, Z. Li, X. Wang, X. Fu, Acta Mater. 55 (2007) 4699–4705.
[14] C. Zhang, Y. Zhu, Chem. Mater. 17 (2005) 3537–3545.
[15] M. Shang, W. Wang, L. Zhou, S. Sun, W. Yin, J. Hazard. Mater. 172 (2009) 338–344.
[16] J. Bi, L. Wu, Z. Li, X. Wang, X. Fu, Mater. Lett. 62 (2008) 155–158.
[17] D. Beydoun, R. Amal, G. Low, S. McEvoy, J. Nanopart. Res. 1 (1999) 439–458.
[18] G. Zhang, J. Yang, S. Zhang, Q. Xiong, B. Huang, J. Wang, W. Gong, J. Hazard. Mater. 172 (2009) 986–992.
[19] L. Wang, W. Wang, M. Shang, S. Sun, W. Yin, J. Ren, J. Zhou, J. Mater. Chem. 20 (2010) 8405–8410.
[20] E.T. Kang, K.G. Neoh, K.L. Tan, Prog. Polym. Sci. 23 (1998) 277–324.
[21] J. Li, L. Zhu, Y. Wu, Y. Harima, A. Zhang, H. Tang, Polymer 47 (2006) 7361–7367.

[22] H. Zhang, R. Zong, J. Zhao, Y. Zhu, Environ. Sci. Technol. 42 (2008) 3803–3807.
[23] H. Zhang, R. Zong, Y. Zhu, J. Phys. Chem. C 113 (2009) 4605–4611.
[24] H. Zhang, Y. Zhu, J. Phys. Chem. C 114 (2010) 5822–5826.
[25] M. Shang, W. Wang, S. Sun, J. Ren, L. Zhou, L. Zhang, J. Phys. Chem. C 113 (2009) 20228–20233.
[26] D. Kong, Langmuir 24 (2008) 5324–5331.
[27] J. Zhang, X. Chen, K. Takanabe, K. Maeda, K. Domen, J.D. Epping, X. Fu, M. Antonietti, X. Wang, Angew. Chem. Int. Ed. 49 (2010) 441–444.
[28] V.V. Atuchin, I.E. Kalabin, V.G. Kesler, N.V. Pervukhina, J. Electron Spectrosc. Relat. Phenom. 142 (2005) 129–134.
[29] G.K.R. Senadeera, T. Kitamura, Y. Wada, S. Yanagida, J. Photochem. Photobiol. A 164 (2004) 61–66.
[30] W. Wu, S. Liang, X. Wang, J. Bi, P. Liu, L. Wu, J. Solid State Chem. 184 (2011) 81–88.
[31] S. Ge, L. Zhang, Environ. Sci. Technol. 45 (2011) 3027–3033.
[32] L. Zhang, K. Wong, D. Zhang, C. Hu, J.C. Yu, C. Chan, P. Wong, Environ. Sci. Technol. 43 (2009) 7883–7888.
[33] A. Fujishima, T.N. Rao, D.A. Tryk, J. Photochem. Photobiol. C 1 (2000) 1–21.
[34] Z. Li, H. Dong, Y. Zhang, T. Dong, X. Wang, J. Li, X. Fu, J. Phys. Chem. C 112 (2008) 16046–16051.